RESERVOIR CHARACTERIZATION AND HISTORY MATCHING OF A DELAWARE SLOPE-BASIN RESERVOIR

F.D. Martin, A. Ouenes, W.W. Weiss
New Mexico Petroleum Recovery and Research Center
New Mexico Institute of Mining and Technology
and Bruce Stubbs
Pecos Petroleum Engineering, Inc.

Abstract

The Delaware formations are submarine channel/fan sands that are difficult to characterize. In this study, new methods have been applied to characterize the East Livingston Ridge Delaware Field. Using well logs, a complex 3-D reservoir model, composed of six layers and a meandering channel, was constructed to represent this geological depositional setup. Due to drastic changes in layer lithologies, determining multiple oil/water contacts and water saturations required a detailed well log interpretation. Using core data and well logs, good correlations between log porosity and core porosity have been obtained. Using the obtained porosity at the wells, geostatistics was applied to estimate the areal porosity distribution in each layer. The permeability distribution was derived by using a k-ϕ correlation obtained from the core data. Since the large-scale 3-D reservoir model, obtained with core data and correlations, does not match the production history, an automatic history matching code was used to estimate large-scale properties.

Production rates of the three phases (oil, gas and water) at each of the 23 wells of this study and the reservoir pressure were history matched using a recently developed automatic history matching algorithm. A detailed reservoir description, including the large-scale k-ϕ correlations, pseudo-relative permeability, and other reservoir engineering parameters were estimated in each layer. The conditioned reservoir model was used to investigate several drilling and/or waterflood schemes for future development of the reservoir.

Background

The U.S. Department of Energy estimates that 42.7 billion barrels (Bbbl) of oil will remain in existing Slope Basin Clastic (SBC) reservoirs unless new and innovative recovery methods are developed and implemented. Of this volume, 5 Bbbl is estimates to reside in the Permian Basin of New Mexico and Texas, and 1 Bbbl will remain in reservoirs that are herein referred to as belonging to the southeast New Mexico Delaware (SENMD) play. A regional map indicating Delaware Mountain Group reservoirs in southeast New Mexico is shown in Fig. 11, and reservoirs located in the play area are identified in Fig. 22 (map courtesy of NM Bureaus of Mines and Mineral Resources) and Table 11. The pools listed have a total original oil in place (OOIP) of 1 Bbbl, an estimated ultimate recovery of 0.1 Bbbl, and estimated 0.9 Bbbl of remaining oil, and a recovery efficiency of only 10%. The low recovery efficiency, together with the large volume of remaining oil, makes this play a significant target for deployment of advanced recovery techniques.

Causes of the low recovery efficiency are primarily early gas breakout and loss of reservoir energy. Suspected causes of the poor recovery include bubblepoint pressures only a few hundred psi below original reservoir pressures and late implementation of pressure maintenance.

The pools in the SENMD play produce from at least two porosity zones scattered within the Bell Canyon, Cherry Canyon, and Brushy Canyon zones of the Delaware Mountain Group of Permian, Guadalupian age. On the northern slope of the Delaware Basin, the pools are composed of a complex and heterogeneous assemblage of depositional environments and depositional textures. The typical structure of these pools is a simple, gentle anticline with no apparent faulting. These characteristics are typical of Permian Basin SBC Pools. Complex vertical and lateral heterogeneity, rather than structural complexity, reduces recovery efficiency in these pools, producing low recovery of the oil in place.

For solution-gas drive reservoirs, all the variables in the material balance equation except the produced gas-oil ratio are a function of pressure and the properties of the reservoir fluids. Since the nature of the reservoir fluids are fixed, the recovery is fixed by the PVT properties of the reservoir fluid and produced gas-oil ratio. Since the cumulative GOR is not significantly affected by rate, the ultimate recovery will not be significantly affected by the production rate.

Because of the increasing GORs, reservoir energy is being expanded rapidly. Therefore, to maximize ultimate recovery, a pressure maintenance project should be considered early in the life of solution gas Delaware pools. Typically, pressure maintenance/waterflooding is not implemented until late in the life of these pools. This results in the reservoirs having high gas saturations, reduced permeability to oil, large voidage, and a reduced chance of an economically successful pressure maintenance project. With the early implementation of pressure maintenance, reservoir pressure can be maintained, a large percentage of gas will remain in solution, permeability to oil will be preserved, and recovery will be maximized.

The key to improving recovery from these types of reservoirs is improved characterization of the spatial distribution of petrophysical properties to provide an accurate characterization of the location of oil saturation, flow properties and fluid properties. After the best reservoir characterization has been achieved, recovery programs can be designed that will target areas with high remaining oil saturation and high recovery potential. Achieving optimum results early in a development program is often critical in the successful continuation of a project. Methods presented here illustrate how key wells can be targeted early and remaining wells can be prioritized accordingly.

The four fundamental activities in reservoir characterization are the following:

1. constructing the geologic framework,

2. quantifying the geologic framework in petrophysical terms,

3. developing and adjusting the geological/petrophysical model for input into reservoir simulators for predicting the distribution of remaining oil saturation, and

4. developing a reservoir description that honors the historical pool production data.

History of the East Livingston Ridge Delaware Field

Strata Production Company and Yates Petroleum Corporation operate the East Livingston Delaware Field which is situated approximately 32 miles southeast of Carlsbad, NM and approximately 30 miles southwest of Hobbs, NM. The field is located in portions of Sections 15,16, 21, and 22 of T-22-S, R-32-E, in Lea County New Mexico.

The discovery well was drilled in late 1991 and the field was officially designated in May of 1992. The field currently is comprised of 24 producing oil wells and one existing salt water disposal well. Through February 1994, the field has produced approximately 802,400 BO, 1,659,000 BW, 726,200 mcfg and is currently averaging 700 BOPD, 2350 BWPD and 1000 mcfgpd.

The field produces primarily from the Brushy Canyon interval of the Permian age Delaware Formation. There are approximately 12 individual producing intervals ranging in depth from approximately 7000 ft below surface to 8500 ft below surface. The majority of the production appears to be coming from two or three individual zones which generally occur between 7100 ft and 7400 ft. These intervals are described as fine-grained to very fine-grained well-consolidated sandstones with porosity between 14 and 20 percent and permeability ranging from less than 1md to as high as 20 md (1–5 md average).

The field is typical of other Brushy Canyon Delaware fields located in Southeast New Mexico and West Texas with multiple stacked sandstone pay zones. Because of its recent discovery, good geologic and engineering information is available for the field. While not as large as the Livingston Ridge and Lost Tank fields (75 wells), the field contains a sufficient number of wells with adequate producing history to provide a good model for other Delaware fields.

The Delaware trend of Southeastern New Mexico and West Texas is one of the most active oil and gas areas in the continental United States. Numerous fields are in their early development, and results of this study could provide critical insight into techniques which could be employed on similar fields in this prolific trend.

Initial Characterization

Viscosity of the 38 degree API oil is 1 cp at 95° F. PVT measurements and relative permeability data from the Livingston Ridge field, six miles to the west, were available and were used in this study. The laboratory k_r curves suggest that the reservoir wettability is intermediate to oil-wet. Initial oil production in this transition zone reservoir is accompanied by water. The lowest initial watercut of the wells in the field was 20%, and the initial production of the majority of the wells included 50% water.

In addition to rock and fluid properties, the data inventory included the monthly oil, gas, and water production histories by well, 24 well logs with porosity, resistivity, and lithology measurements, and 360 sidewall cores from 16 wells. History of the static reservoir pressure was not complete. The permeability at the well locations could be estimated with some confidence; however, interwell permeabilities were estimated by history matching the production performance of the individual wells.

The geological 3-D cartoon in Fig. 3 provides a conceptual view of the Brushy Canyon Reservoir. The lower sediments include a variable permeability channel through the "D", "D1", and "D2" sands while the upper "A", "B", and "C" sands are unbroken deposits. Analyses of the openhole logs provided the initial petrophysical description of the geological units depicted in the cartoon. A 2.67 gm/cc matrix density was estimated by tuning the density log to the measured sidewall core porosity. The intercept of a Pickett plot (logarithmic graph of resistivity versus density porosity) was used to estimate a 0.03 ohm-meter connate water resistivity, a cementation exponent of 2.0 , and a 1.0 tortuosity factor. These values, when used to calculate water saturations, resulted in values greater than 100% and occasional oil-water contacts above the oil producing zones within the individual layers.

The problem of the 100% plus water saturation was solved by substituting the difference of the recorded bulk density and the matrix density for the density-porosity values in a Pickett plot. The matrix density values were adjusted by trial and error until a straight line was observed. The straight line matrix density was 2.66 gm/cc. The inverse of the slope of a Pickett plot with the corrected matrix density produced a cementation exponent of 1.9. These values resulted in water saturations less than 100%, slightly reduced bulk volume water values, and a maximum water saturation value of 66% for determination of the oil-water contact. Pertinent reservoir data provided in Table 2 includes average porosity, permeability and saturations.

Well logs were used to construct a view of the structure by layer. A view of the top of the "D2" sand is shown in Fig. 4. Notice the presence of the channel through the center of the picture with breaks in the boundaries along the channel. A creative application of kriging was used to locate the channel boundaries. The depth of the layers and their thicknesses were determined from the logs and were used to prepare a kriged isopach for each layer. The boundaries of the channel were obtained by analyzing the isopach map of the top of layer "D." At the channel location, the top of the "D" layer was higher than the average depth of the layer. As a result, the kriged map showing the top of the "D" layer exhibits a clear "bump" at the channel location. All the gridblocks located at the bump were considered as representing the channel.

Geologic model

Using the log data and kriging, the top structure and thickness of each layer was found. The total thickness of the channel was broken into three parts, the first being connected to the layer "D", the second thickness connected with layer "D1", and the last part of the channel connected to layer "D2" (Fig. 3). The available sidewall cores were used to find, at the core scale, the relation between porosity and permeability. All the data were fitted using the relation:

$$k = 10^{a\phi - b}$$

The analysis of these correlations revealed the existence of at least seven lithologies. Each layer has a specific lithology leading to the permeability-porosity coefficients shown in Table 2, and the channel itself exhibited two types of lithologies. For simplicity, the channel was represented as a single lithofacies. The porosity varied little within a given lithological zone, but the permeability-porosity correlation varied significantly from one zone to another as can be seen in Table 2. These observations lead to the following strategy in characterizing the dynamic performance of the reservoir. The porosity distribution obtained by kriging in each lithological zone was considered reliable and remained unchanged during the history match. However, the coefficients used in the porosity-permeability correlations as well as the relative permeabities in each lithological zone were adjusted during the automatic history match. The geologic model, which honors all the log information, lead to an estimation of an original oil in place of 231 millions barrels of oil. More than half of the OOIP is found in the lower zone described as "D2" layer. The remainder is primarily found in the upper layers ("A","B", and "C"). Based on the geologic model, reservoir simulation was used to history match the production.

Automatic History Matching

The reservoir model was discretized into seven layers. Each layer was represented by 462 gridblocks (21 × 22) to cover an area of about two sections. The gridblocks are cubes with a length of L=400 ft, and the thickness, h, varied over the reservoir. The solution gas drive reservoir had an average L/h ratio of 80, which is satisfactory for simulation purposes. The total number of gridblocks in the reservoir model is 3,234, and the history match represented a period of 23 months of primary production. One simulation run required an average of six minutes, wall-clock time. The oil rate was used as the boundary condition, and the simulator predicted the water rate, gas rate, and the pressure. Unfortunately, complete pressure data were not available, therefore, production was the only field data included in the error to be minimized by a complex computer code. Briefly speaking, an iterative process is used to adjust reservoir parameters automatically until the production history is correctly matched. At each iteration, the values of the reservoir parameters are adjusted, a full reservoir simulation is run, and the error between simulated and field production history is computed. If this error is reduced (in the simulated annealing sense) then the values tested are kept for further adjustments.

The major reservoir parameters adjusted automatically in this study were geological and petrophysical. For each lithological zone, the optimization algorithm found the two parameters, a and b, used in the porosity-permeability correlation. There are two main justifications for this approach. First, in each lithological zone, there are limited core data that may lead to a poor correlation. For the seven lithological zones, the correlation coefficient was ranging from 0.5 to 0.7, except for layer "A" where the correlation coefficient was 0.92. The second factor is related to the fact that permeability measured on a core is not representative of a permeability of a gridblock that is 400 ft long (upscaling problem). Usually, the core permeability is greater than the gridblock permeability. In addition to permeability estimation, the optimization routine searched for various parameters describing relative permeability curves for oil, water, and gas. The analytical expressions used to describe these curves are standard power law:

$$k_{r_w} = (k_{r_w})^{max} \left(\frac{S_w - S_{w_i}}{1 - S_{w_i} - S_{o_r}} \right)^{ex_w}$$

The estimation parameters are the endpoint kr_w^{max}, and the power ex^w. Similar functions are used for oil and gas relative permeability curves. The history matching task was stopped when a reasonable match was obtained (Figs. 5 and 6). A major difficulty was the matching of water production which included out of zone water from perforated wet zones and out-of-zone hydraulic fracturing. These completion problems resulted in a large amount of water production and were difficult to model. The excess water resulting from non oil-bearing zones was represented by a layer which contains water and no moveable oil. The properties of this water bearing zone were adjusted to account for the excess of water resulting from unknown completion factors. The reliability of the model was tested by forecasting eight months production which was not included in the history match. The results of the forecast as compared to the actual production is shown in Figs. 5 and 6. The well labeled #23 was not included in the history match and was purely a forecast. Another verification of the model consisted of recent buildup tests on four wells. The comparison of forecasted pressures at the four well locations with the obtained field pressures indicates that the reservoir model is correctly simulating the dynamic reservoir behavior. Using the conditioned model, various reservoir development strategies were investigated.

Reservoir Management Strategies

Infill Drilling

Using the reservoir model and the forecasted pressure and oil distribution, an infill criterion map was computed. The infill criterion characterizes each gridblock in a quantitative manner for the suitability of an infill well. The infill criterion uses four parameters obtained from the reservoir model. The first parameter is the pressure P(x,y,z), obtained after simulating 35 months of primary production (November 1994). The second parameter is the oil saturation S_o(x,y,z) obtained in a similar way. The third parameter is the pore volume PV(x,y,z) which was obtained by geostatistical modeling. The fourth parameter is the permeability k(x,y,z) of each gridblock obtained after finding the correct coefficients for the permeability-porosity correlation. The criterion CR(x,y,z) can be written as:

$$CR(x,y,z) = P(x,y,z)S_o(x,y,z)PV(x,y,z)k(x,y,z)$$

After obtaining the infill criterion in each gridblock of the 3-D model, the values of CR(x,y,z) are averaged in the vertical direction to obtain a 2-D infill drilling criterion map. When examining this map, it is apparent that the only potential for infill wells is located in the south of the reservoir. Four potential infill wells (Wells 24, 25, 26 and 27) were selected as shown in Fig. 7, and their performance forecasted. The forecasted oil of the favorable infill well located in the south (Well # 24) is shown in Fig. 8. The ultimate primary recovery of this well is about 40,000 of barrels of oil.

The forecasted oil rate of the well located in the north part of the reservoir (Well # 27) is shown in Fig. 9. Ultimate primary recovery for Well # 27 is about 24,000 of barrels of oil. These forecasts suggest that infill drilling at these locations in the East Livingston Ridge field may be marginal with current oil prices. As a consequence, another reservoir management strategy was explored.

Waterflooding

After an additional five years of primary including the four infill wells, a waterflood with 11 injection wells was simulated beginning in 1999. The line-drive pattern (see Fig. 7) with injection limited to the D, D1, and D2 zones was simulated. The water injection rate was 10,000 bbl/month into each well for more than three years. The composite unit production is shown in Fig. 10. For the line-drive pattern used in the simulation, the production of an additional 150,000 barrels suggests that waterflooding may be a viable management strategy. Additional simulations of a waterflood beginning earlier in the depletion of the field are underway, and development strategies using other patterns are under investigation for optimizing oil recovery.

Conclusions

1. A novel application of kriging was used to define the boundaries of a channel in a complex submarine fan geological setting.
2. A recently developed automatic history matching method was used to determine that half of the oil production from the East Livingston Ridge Delaware reservoir originated from a single layer, the "D2." The method automatically adjusted the porosity-permeability correlation and estimated the proper relative permeability power-law parameters.
3. Infill drilling is a marginal prospect with today's business climate.
4. Waterflooding may be a viable management strategy, especially if oil prices increase.

Acknowledgements

The authors would like to acknowledge Mark Murphy, and John Worrall from Strata Production, and Robert Fant, Dave Boneau, John McRae, and Denise Fly from Yates Petroleum Corporation.

Table 1 - Regional Delaware Mountain Group
Slope Basin Clastic Reservoirs, S.E. New Mexico

1. Washington Ranch
2. Serpentine Bends
3. Glenn
4. Welch
5. Tecolote Peak
6. Tecolote Peak
7. Red Bluff
8. SW Sulphate
9. PJ
10. Sulphate Draw
11. W. Malaga
12. Black River
13. Elbow Canyon
14. Dark Canyon
15. East Dark Canyon
16. West Dark Canyon
17. Brynes
18. Forehand Ranch
19. Happy Valley
20. Cass Draw
21. Filaree Dome
22. S Carlsbad (Del)
23. W Carlsbad
24 S Carlsbad (CC)
25. WYE
26. Loving
27. Herradura Bend
28. N. Willow Lake
29. Revelation
30. E. Herradura Bend
31. E. Loving
32. S. Loving
33. N. Malaga
34. S Culebra Bluff
35. Malago
36. Ceder Canyon
37. Willow Lake
38. Indian Head
39. East Indian Draw
40. Esperanza
41. Indian Flats
42. Fenton
43. US
44. NW Fenton
45. La Huerta
46. Foster Draw
47. Carlsbad
48. Scanlon
49. Golden Lane
50. S Golden Lane
51. E Cat Claw Draw
52. Cat Claw Draw
53. Nash Draw
54. Forty Niner Ridge
55. SE Quahuda Ridge
56. 57 Quahuda Ridge
57. Cabin Lake
58. Lost Tank
59. NE Livingston Ridge
60. Livingston Ridge
61. SE Livingston Ridge
62. E Livingston Ridge
63. W Red Tank
64. S Red Tank
65. Bootleg Ridge
66. Dagger Lake
67. NW Bootleg Ridge
68. N Legg
69. Bilbrey
70. Los Medanos
71. W Sand Dunes
72. S Livingston Ridge
73. E Sand Dunes
74. S Sand Dunes
75. Dogtown Draw
76. SW Poker Lake
77. W Poker Lake
78. Poker Lake
79. N Poker Lake
80. E Poker Lake
81. Cotton Draw
82. S Poker Lake
83. S. Cotton Draw
84. W Corral Canyon
85. Corral Canyon
86. N Brushy Draw
87. Brushy Draw
88. E Brushy Draw
89. N. Ross Draw
90. W Ross Draw
91. Ross Draw
92. E Ross Draw

93. N Mason
94. Battleaxe
95. E Mason
96. El Mar
97. Rattlesnake Flat
98. E El Mar
99. Bradley
100. Salado Draw
101. Jennings
102. Big Sinks
103. Paduca
104. E Paduca
105. Ingle Wells
106. W Tristle Draw
107. Diamond Trail
108. Cruz
109. Tristle Draw
110. N Paduca
111. E Tristle Draw
112. Double X
113. Triple X
114. Bell Lake
115. N Bell Lake
116. Antelope Ridge
117. S Antelope Ridge
118. Grama Ridge
119. Jal West
120. Penlon
121. Combs
122. Avalon
123. Russell
124. Burton
125. E Burton
126. Outpost
127. Fadeway Ridge
128. Parkway
129. Santo Nino
130. Big Eddy
131. Maroon Cliff
132. Parallel
133. S Lusk
134. W Lusk
135. Lusk
136. N Lusk
137. W Tonto
138. Gem
139. Salt Lake
140. Hackberry
141. Crazy Horse
142. E Lusk
143. Geronimo
144. Hat Mesa
145. Shugrat
146. E Shugrat
147. N Young
148. Corbin
149. Querecho Plain
150. N Querecho Plain
151. W Corbin Plain
152. EK
153. E Gem
154. Quail Ridge
155. Lea
156. NE Lea
157. Mid Vacuum
158. Reeves
159. W Lovington

Table 2 - Reservoir Properties

Zone	Average Thickness,ft	Average Porosity,%	Permeability Exponents	Swi %	Oil-Water Contact ft. sea level	
			a	b		
A	2.45	16.3	0.217	2.86	26.6	-3320
B	6.24	15.9	0.257	3.26	37.6	-3360
C	5.43	14			32.1	-3430
D	4.97	16.2	0.183	2.22	66.9	-3509
D1	9.17	15.4	0.242	2.89	66.2	-3545
D2	10.1	17	0.242	2.89	38.2	-3595
channel		15.8	0.744	10.2	46.9	NA

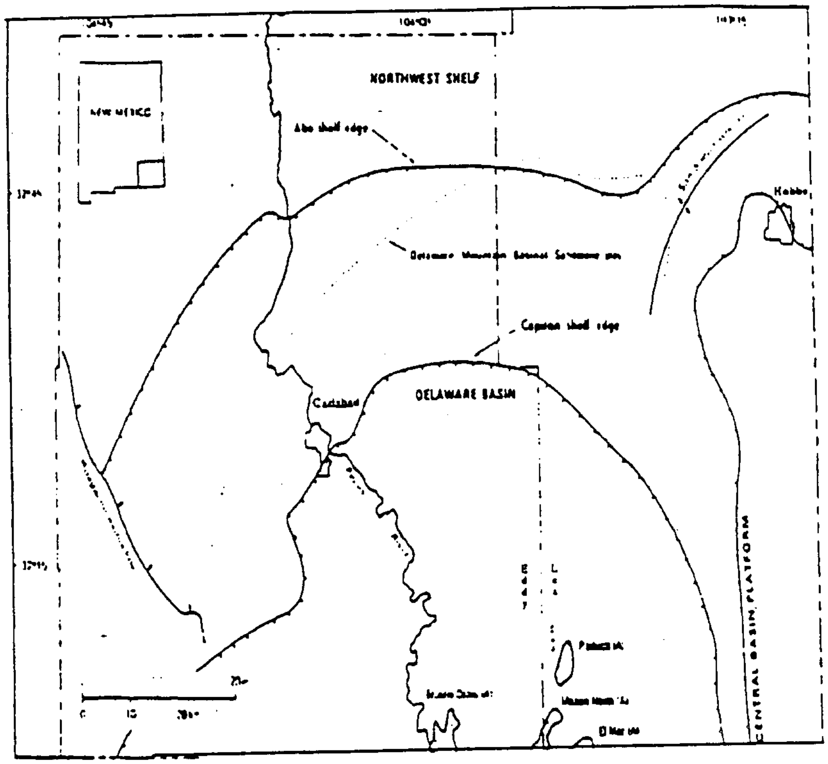

Figure 1 - TORIS Class III Database,
Delaware Pool Location

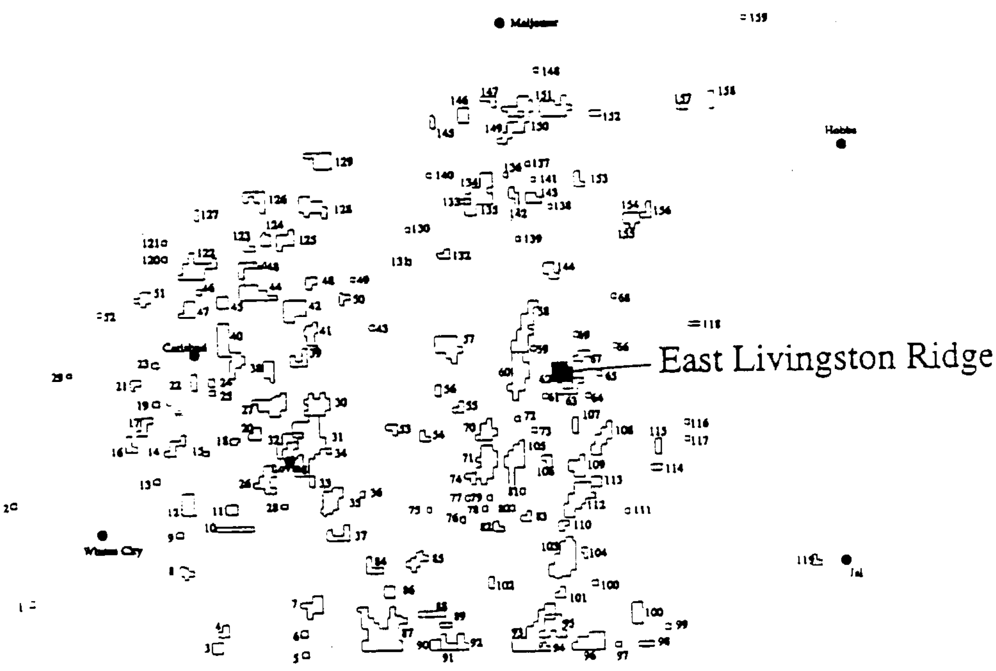

Figure 2 - Location of ELR and surrounding fields

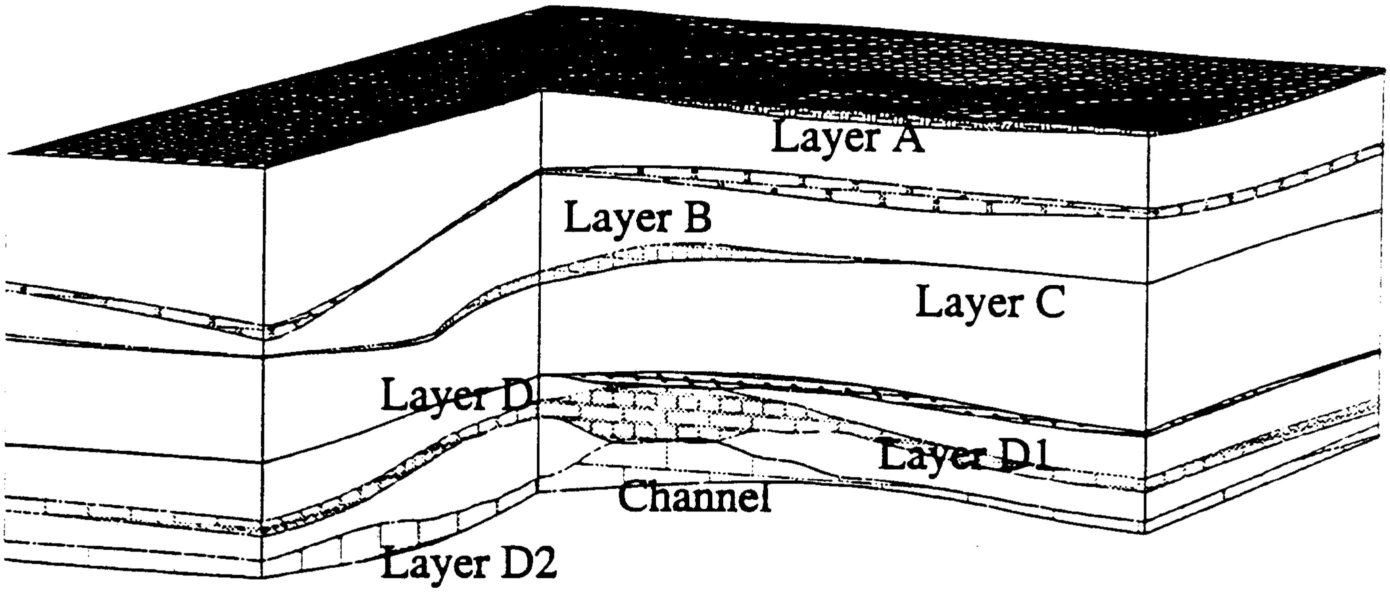

Figure 3 - Geologic model of ELR

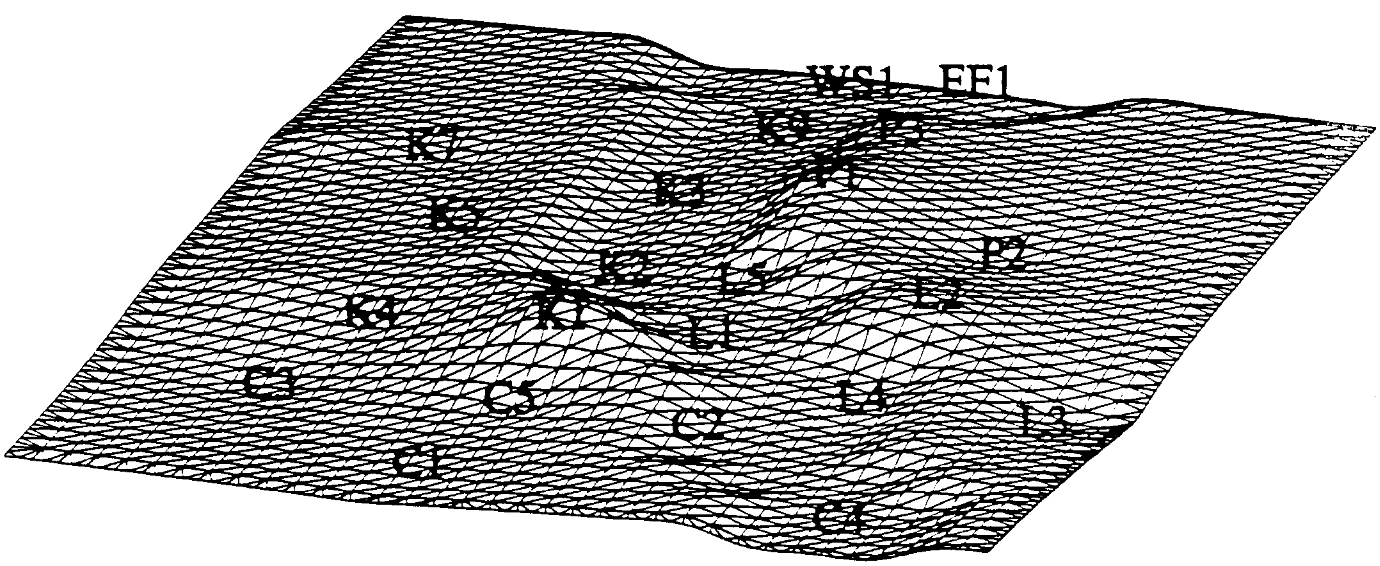

Figure 4 - Well locations shown on the top of D2 layer

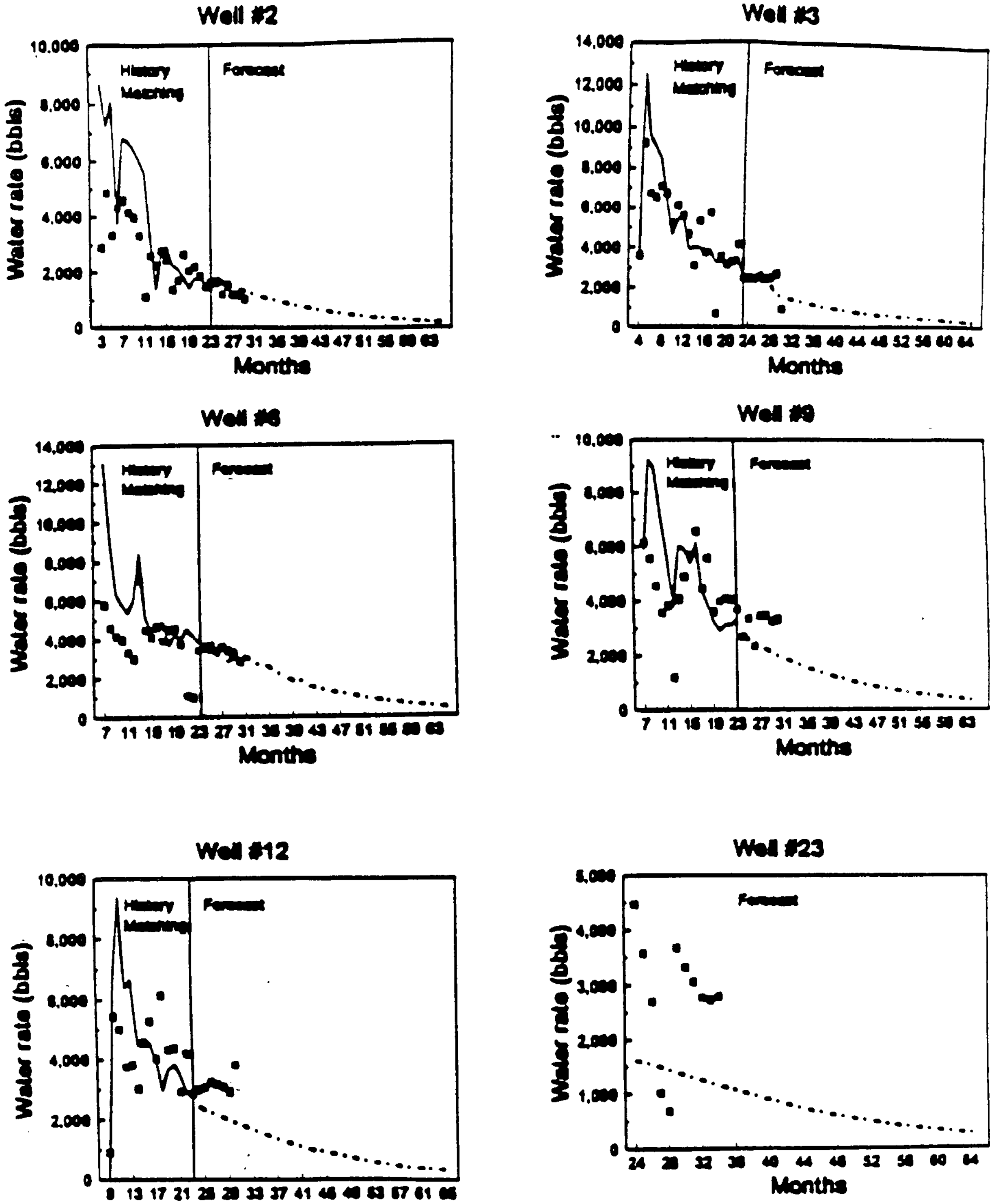

Figure 5 - Matching and forecasting primary water rate

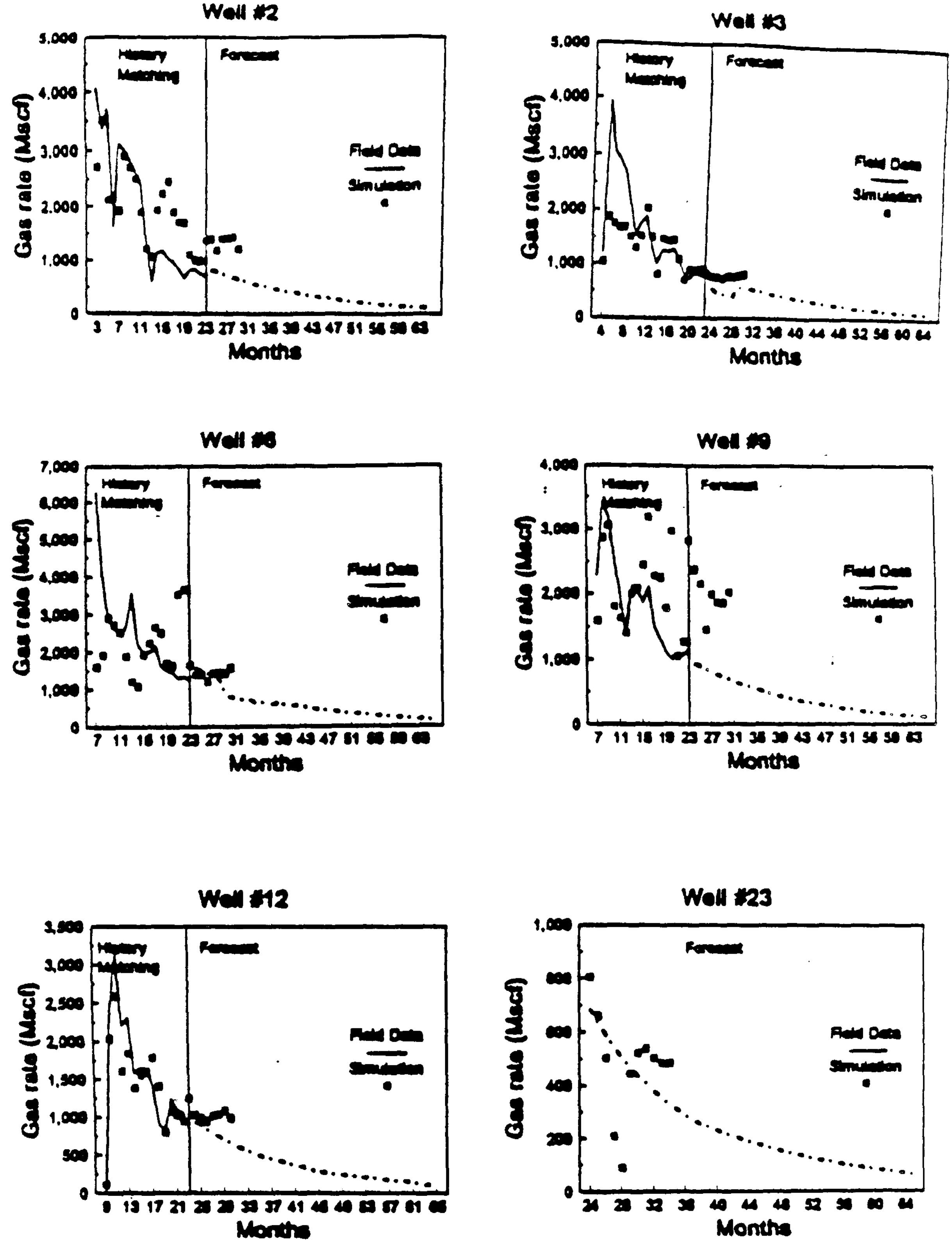

Figure 6 - Matching and forecasting primary gas rate

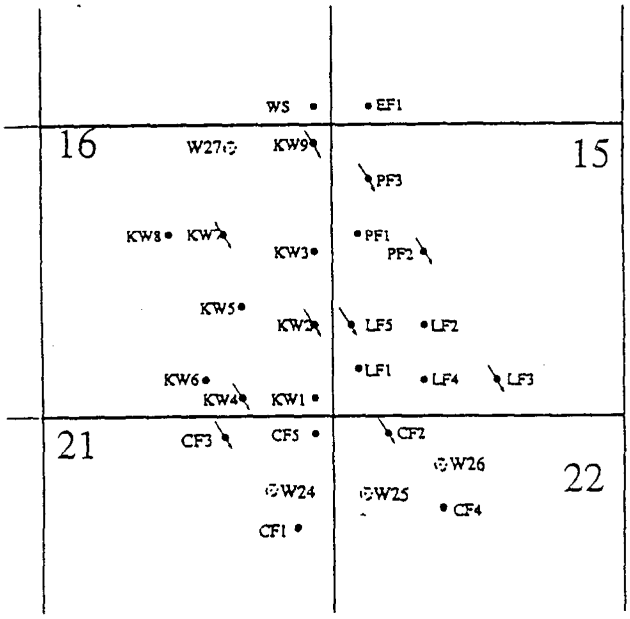

Figure 7 - Well locations and planned infill wells and injectors

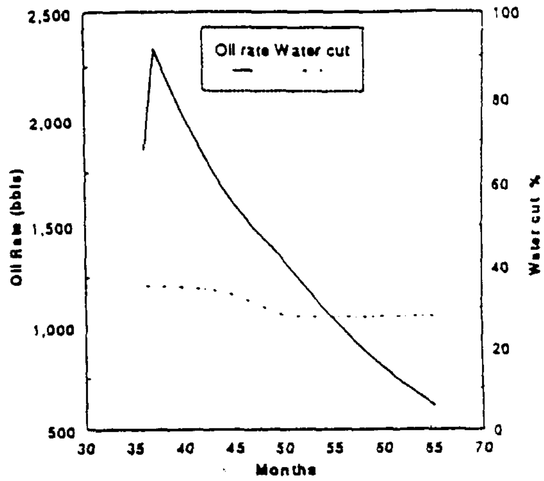

Figure 8 - Performance of infill well 24

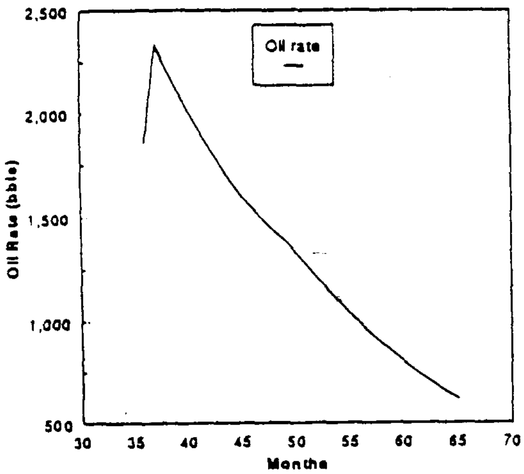

Figure 9 - Performance of infill well 27

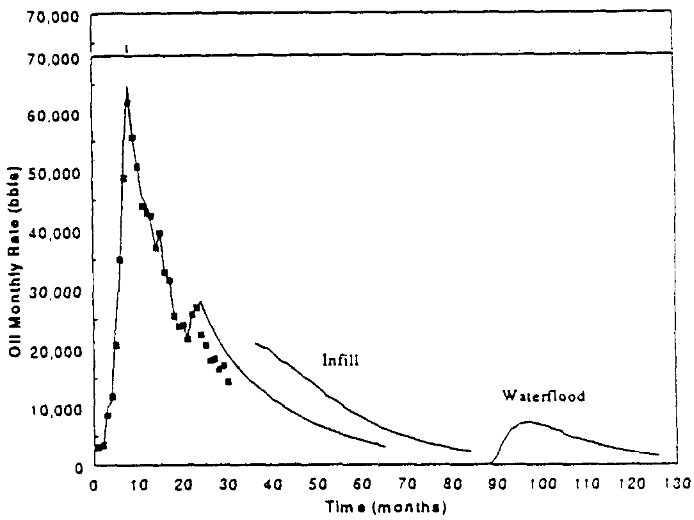

Figure 10 - Field Performance